Journal of Power Sources 407 (2018) 14–22

Contents lists available at ScienceDirect

Journal of Power Sources

journal homepage: www.elsevier.com/locate/jpowsour

Preparation and optimization of miniaturized radioisotope thermoelectric generator based on concentric filament architecture

Kai Liu[a], Xiaobin Tang[a,b,*], Yunpeng Liu[a,b], Zhiheng Xu[a], Zicheng Yuan[a], Junqin Li[a], Zhengrong Zhang[a]

[a] Department of Nuclear Science and Engineering, Nanjing University of Aeronautics and Astronautics, Nanjing, 210016, China
[b] Jiangsu Key Laboratory of Material and Technology for Energy Conversion, China

HIGHLIGHTS

- Miniaturized RTG prototype based on concentric filament architecture was prepared.
- The simulation feasibility was well verified by experimental and analog comparison.
- The RTG's structural parameters are rigorously optimized by finite element method.
- The novel structural design and optimization ideas have a good application value.

ARTICLE INFO

Keywords:
Concentric filament architecture
Radioisotope thermoelectric generator
Finite element analysis method
Structural optimization

ABSTRACT

Given independent and flexible power supply requirements of space apparatus, miniaturized radioisotope thermoelectric generators are currently playing an increasing role in space power systems. This study creatively proposes a miniaturized integrated-design radioisotope thermoelectric generator based on concentric filament architecture and is the first to formulate a practical battery entity. When heat source temperature is 398.15 K, the maximum open-circuit voltage of 418.82 mV and the maximum output power of 150.95 μW are obtained. The COMSOL is used to simulate precisely the thermoelectric conversion process and optimize the structural size of the radioisotope thermoelectric generator. The optimal results are obtained when the ratio of N- to P-type circle radius and the thermoelectric filament's length are 0.1 and 20 mm, respectively. In this case, the battery obtains the maximum output power of 423.50 μW and open-circuit voltage of 605.84 mV when heat source temperature is 398.15 K. When the thermoelectric filament's curvature is 170°, the electrical density value increases more remarkably than that of 0°. Its effective open-circuit voltage density and output power density are 73.79 mV cm^{-3} and 53.76 μW cm^{-3}, respectively. The optimized miniaturized radioisotope thermoelectric generator is able to provide power support for space microelectronic devices.

1. Introduction

Space exploration is a scientific observation and measurement that involves a large number of electrical loads. Hence, detecting massive parameters, such as space particle flux and magnetic field intensity, is generally necessary. Relevant scientific instruments, such as radioactivity detection, magnetometer, and cosmic dust analyzer, have also increased with the escalation in detection tasks. Independent and flexible power supply modes for space apparatus require high and effective electrical energy output of power equipment [1,2]. The radioisotope thermoelectric generator (RTG) converts decay heat from radioisotopes into electrical energy by using thermoelectric devices. It has numerous advantages, such as high reliability, long lifetime, and minimal environmental impact [3,4]. With the miniaturization and increasing application of scientific experimental equipment, research on the miniature RTG is also growing. Therefore, an ideal application prospect for RTG is worth pursuing in spacecraft power supply [5].

Structural design and practical preparation of miniaturized RTG are the current research hotspot. Drinker et al. prepared a π-type thermoelectric generator with slender thermocouples and obtained a maximum open-circuit voltage (V_{oc}) of 5.1 V and an output power (P_{out}) of 82 mW with temperature difference of 300 K [6,7]. However, the thermoelectric leg was brittle due to the small aspect ratio, resulting in several difficulties in fabricating thermoelectric devices. Whalen et al.

* Corresponding author. Department of Nuclear Science and Engineering, Nanjing University of Aeronautics and Astronautics, Nanjing, 210016, China.
E-mail address: tangxiaobin@nuaa.edu.cn (X. Tang).

https://doi.org/10.1016/j.jpowsour.2018.10.052
Received 5 September 2018; Received in revised form 7 October 2018; Accepted 14 October 2018
0378-7753/

Nomenclature

A	P-/N-type cross-sectional area of a thermoelectric filament (cm^2)
J	Current density in the RTG ($J \cdot cm^{-2}$)
L	Length of a thermoelectric filament (mm)
P_{out}	Output power of the RTG (W)
P_{max}	Maximum output power of the RTG (W)
Q	Heat flux in the RTG ($J \cdot cm^{-2}$)
Q	Energy accumulation in the RTG (J)
R	External load resistance in the RTG (Ω)
R_r	Internal resistance in the RTG (Ω)
T_h	Surface temperature of the heat source (K)
ΔT	Temperature difference of the hot and cold sides of the RTG (K)
V_{oc}	Open-circuit voltage of the RTG (V)
V_{eff}	Effective volume of thermoelectric devices (cm^3)
r_1/r_3	Ratio of N-to-P-type circle radius
ν_{eff}	Effective open-circuit voltage density of the RTG ($V \cdot cm^{-3}$)
ρ_{eff}	Effective maximum output power density of the RTG ($W \cdot cm^{-3}$)
θ	Curvature of the thermoelectric filament (°)
α	Seebeck coefficient ($\mu V \cdot K^{-1}$)
σ	Electrical conductivity ($S \cdot m^{-1}$)
κ	Thermal conductivity ($W \cdot m^{-1} \cdot K^{-1}$)

designed a cylindrical small-scale thermoelectric battery with an V_{oc} of 82 mV and a Maximum output power (P_{max}) of 450 μW, while the heat source power was 150 mW [8]. Its structure could be further optimized yet. Several researchers have also utilized the microelectromechanical equipment or the pinpoint technique to prepare micro thermoelectric generators in a small volume. But those thermoelectric devices usually have a considerably large internal resistance and poor thermoelectric conversion efficiency [9–11]. Hence, they cannot provide good practicability in space power supply. To address the low-power and high-voltage requirements of aerospace microelectronic devices, we designed a novel concentric filament architecture for a thermoelectric generator. In comparison with traditional π-type structure, the thermoelectric filament's open-circuit voltage was 2.4 times, and the output power remained unchanged while reducing the thermoelectric material by 28%. This structure remarkably improved the output performance of the thermoelectric devices [12].

Generally, the performance of RTGs can be remarkably improved by optimizing its structure and size. Moreover, the electrical performance of miniaturized thermoelectric generators is more closely related to its structure and size than that of large thermoelectric generators [13–15]. Chen et al. used the Taguchi method to optimize multiple parameters, including the length and width of heat sink. Through analysis, the output power of thermoelectric generator system was further improved by approximately 6% [16]. Shen et al. analyzed the annular thermoelectric couple's structural parameters and obtained the extremums of dimensionless output power and efficiency [17]. In our previous work, the concentric thermoelectric filament with good electrical output was initially proposed, and its feasibility in the thermoelectric device has been successfully verified via experiments. On the basis of our previous study, we focused on the practical application and optimization design of thermoelectric filaments in the present work from the holistic application perspective. In accordance with the characteristics of the thermoelectric filament, a miniaturized high-performance RTG was prepared. The structural parameters and overall volume of the RTG were then optimized using the finite element analysis method. The method could effectively increase the electrical performance of a

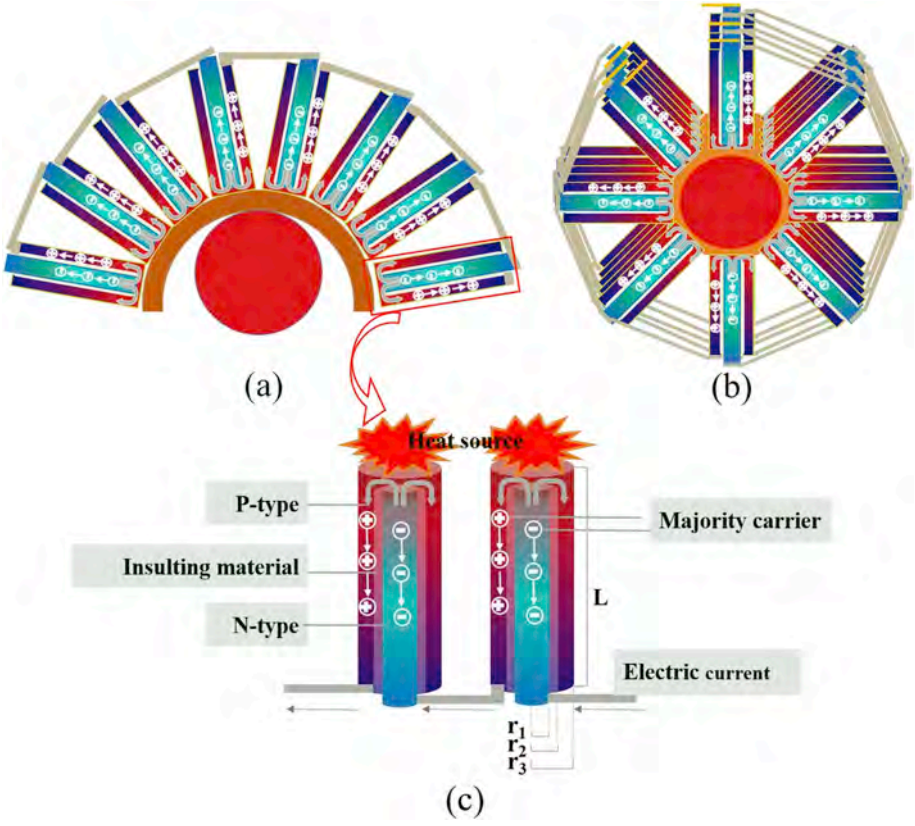

Fig. 1. Miniaturized RTG: (a) concentric filament architecture, (b) sectional view of a thermoelectric filament, and (c) monolithic construction.

battery and meet the power demand of space science equipment.

2. Structural design and steady analysis

The structure of the miniaturized RTG based on concentric filament architecture is shown in Fig. 1. The middle part of the battery is a cylindrical radioisotope heat source, and the outer layer is a heat conduction material. The multilayer radial thermoelectric modules are stacked around the radioisotope source and connected with each other in series. Each of radial thermoelectric modules consists of a plurality of thermoelectric filaments. The P-/N-type thermoelectric materials in a thermoelectric filament are isolated using an insulating material. The electric current initially flows through the inner N-ring into the outer P-ring and then flows out. The edge of the outer P-type ring is connected with the end point of the N-type in another filament through the copper wire. The outer radius of the P-/N-type material and the insulating layer is r_3, r_1, and r_2, respectively. The length of the thermoelectric filament is L. The dimension parameters of thermoelectric filaments are tightly linked to the distribution of temperature and electric potential fields that finally influence the electrical output of the battery. In the theoretical analysis, the following initial and boundary conditions of thermoelectric conversion process are initially examined.

- The surface temperature of the radioisotope heat source is a fixed value.
- The ambient and initial temperatures are set to 293.15 K. The sample is placed in the natural air convection environment with a convective coefficient of 6 $W m^{-2} K^{-1}$.
- The thermal and electrical insulations are involved with all boundary parts of the battery.
- The electrical and thermal contact resistances between thermoelectric filaments and electrodes are negligible.

The internal relations among parameters, such as temperature difference (ΔT), internal resistance (R_r), and structural parameters, are introduced by importing r_1, r_2, r_3, and L.

$$\Delta T = \int \frac{q}{\lambda\cdot((r_3^2 - r_2^2)\pi + r_1^2\pi)} dl \tag{1}$$

$$R_r = \frac{\rho_p l_p}{(r_3^2 - r_2^2)\pi} + \frac{\rho_n l_n}{r_1^2\pi} \tag{2}$$

The coupling analysis of multiple physical fields, including thermodynamic and electric fields, is conducted. The equation of current density (J), heat flux (q) related to electric potential (V), material parameters, and temperature (T) are expressed as follows:

$$-J = \sigma\cdot\nabla V + \sigma\alpha\cdot\nabla T \tag{3}$$

$$q = -\kappa\cdot\nabla T + T\alpha\cdot J \tag{4}$$

where σ, α, and κ represent the electrical conductivity, Seebeck coefficient, and thermal conductivity, respectively. In a steady state, J is free to diverge.

$$\nabla\cdot J = 0 \tag{5}$$

$$\nabla\cdot q = \nabla\cdot(VJ) \tag{6}$$

At this stage, the energy accumulation (Q) must be 0.

$$Q = \nabla\cdot(\kappa\cdot\nabla T) - \nabla((V + T\cdot a)\times J) = 0 \tag{7}$$

When determining the q value of the radioisotope heat source (i.e., the temperature of the heat source is determined), the internal relations of V and T with respect to the material parameters, such as σ and κ, are established. For the entire battery, V_{oc} and P_{out} are calculated as follows:

$$V_{oc} = \alpha \times \Delta T n \tag{8}$$

$$P_{out} = \frac{V^2}{(R + R_r)^2}\cdot R \tag{9}$$

$$v_{eff} = V_{oc}/V_{eff} \tag{10}$$

$$\rho_{eff} = P_{out}/V_{eff} \tag{11}$$

where n is the number of P-/N-type legs in the thermoelectric module; R is the external load resistance; and V_{eff} is the effective volume of thermoelectric devices, which include the thickness and diameter of the thermoelectric device without the interspace of two layers. In addition, P_{max} is obtained if $R = R_r$. v_{out} and ρ_{out} are voltage and power densities, respectively. From the analysis of these equations, the electrical output of the RTG is closely linked with L, P-/N-type cross-sectional area (A), and V_{eff}. The electrical performance of the device will be considerably improved by optimizing these values.

3. Experimental preparation and test

3.1. Preparation and testing process

A miniaturized RTG is usually prepared using a ^{238}Pu heat source and homemade tellurium bismuth thermoelectric modules. $^{238}PuO_2$ has a high specific power of 0.406 W g^{-1} (or 3.94 W cm^{-3}) and a long half-life of 87 a, which is an ideal heat source for the RTG. According to relevant parameters of existing miniaturized RTG (Table 1) and the applicable temperature range of thermoelectric materials, we intended to use less than 8.62 g $^{238}PuO_2$ to provide a heat source temperature (T_h) range of 298.15–398.15 K [18,19]. In the actual fabrication, the electric heating rod of aluminum oxide (with a volume of 0.96 cm^3 and an internal resistance of 6.4 Ω) was considered to be the simulated heat source to provide a specific heat source temperature [7,20,21]. P-type Bi_2Te_3 paint and N-type constantan wire were selected as the thermoelectric materials for preparing the thermoelectric filaments, which was conducted using the brush coating method; the detail of the preparation is shown in Supplementary Information 1 [10]. The constantan wire has excellent toughness and is currently one of the best N-type metal thermoelectric materials [22]. Thus, thermoelectric filaments could be formulated into various bending degrees. Eight thermoelectric filaments were arranged on the adiabatic substrate with a radial layout. The filaments were connected using copper wire and conductive silver paste. Five layers radial thermoelectric devices were stacked and connected in series, then placed in an aluminum case and encapsulated using the aluminum silicate wool (1260-type with a thermal conductivity of 0.03 W $m^{-1} K^{-1}$). The prepared miniaturized RTG, whose diameter is 65 mm, is shown in Fig. 2. Its internal resistance is 237.14 Ω at room temperature (293.15 K).

The electrical performance of the RTG was tested using a parameter analyzer (Keithley 4200 SCS) at an ambient temperature of 293.15 K (Fig. 3). The input electrical parameters of an electric heating rod, similar to the electric voltage and current, were controlled to provide a stable temperature (298.15–398.15 K). The preheating time was approximately 30 min before beginning the formal test to obtain a stable internal temperature field and improve the accuracy of measurement

Table 1
Basic parameters of the miniaturized RTG [23,24].

Type of RTG	Heat power (W)	Heat source mass (g)	Heat source temperature (K)	Service life (a)
RTG-1/0.5	0.22	0.54	353.15	10
RTG-2.5/2.5	0.6	1.48	373.15	10
RTG-20/30	0.15	3.94	403.15	10
RTG-50/12	3.5	8.62	423.15	10

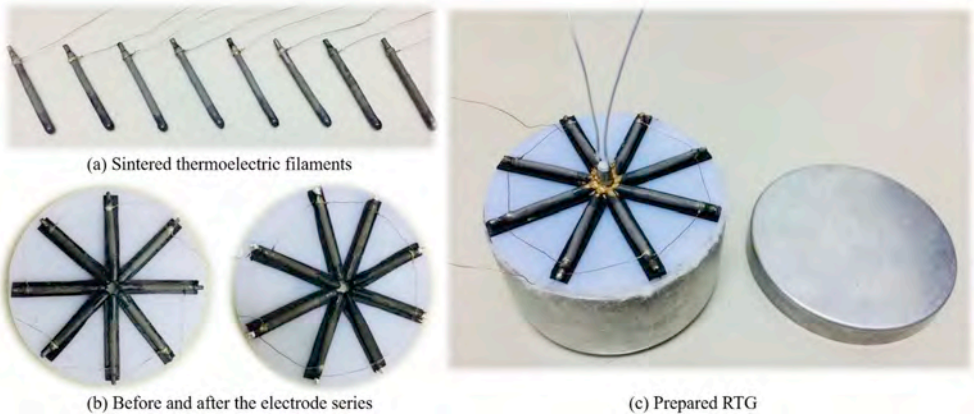

Fig. 2. (a) Sintered thermoelectric filaments, (b) before and after series connection of the electrode, and (c) prepared RTG.

data. The real-time temperatures of the hot and cold sides of the thermoelectric filaments were measured using a temperature sensor (R7100).

3.2. Measurement of structural size and material parameters

After preparing the thermoelectric filaments, the relevant dimensions in Table 2 were tested. The diameter of the prepared thermoelectric filament is approximately 2.54 ± 0.05 mm with a length of 30 mm. The P-type bulk samples were prepared using the same thermoelectric paint ratio and sintering method to characterize the electrical properties of the thermoelectric materials. Similarly, the N-type constantan with certain thickness was adopted to measure the corresponding parameters. The relevant instruments were used to determine the Seebeck coefficient (self-built testing platform, Agilent 34970A), electrical conductivity (Hall effect system), and thermal conductivity (DRL-III thermal conductivity test system) of the P-/N-type thermoelectric materials in the range of 298.15–398.15 K. Supplementary Information 2 introduces the test process of the Seebeck coefficient. The performance curve of the P-/N-type thermoelectric material of the temperature are shown in Fig. 4. The Seebeck coefficient of the P-type thermoelectric material is in the range of 136.06–162.54 μV K^{-1}. When the measurement temperature is increased, the Seebeck coefficient initially increases and then decreases. The maximum value is 162.54 μV K^{-1} at 323.15 K. The thermoelectric paint contain organic solvents and have low thermal conductivity. Thus, a large temperature difference could be obtained in a macroscopic aspect, although electrical conductivity is limited. The P-type electrical and thermal conductivities increase slightly with the increase in test temperature. The constantan is one of the best N-type metal thermoelectric materials, and its measured range is 33.37–45.74 μV K^{-1}. Moreover, it has excellent conductivity and can effectively reduce the internal resistance of the entire battery. The relevant test results of an N-type thermoelectric material are close to the data in the existing literature, thereby reflecting the credibility of the test results [19].

Table 2
Related parameters of the structural size for the thermoelectric filaments and RTG.

Dimension parameters	Internal diameter r_1 (mm)	Middle diameter r_2 (mm)	Outer diameter r_3 (mm)	Height L (mm)
Thermoelectric filament	1.50	1.85	2.54	30
Dimension parameters	**Diameter (mm)**	**Height (mm)**	**Whole volume V_{all} (cm^3)**	**Effective volume V_{eff} (cm^3)**
Miniaturized RTG	65	50	165.83	39.57

3.3. Measurement of electrical output performance

The surface temperature of the heat source was maintained at 298.15–398.15 K by controlling the input electrical parameters of electric heating rod, similar to electric voltage and current. The Volt-Ampere (V–I) characteristic curve of the RTG presents a good linear variation, as shown in Fig. 5a. When T_h increases from 298.15 K to 398.15 K, the thermoelectric filament exploits the advantage of small aspect ratio to the full. The temperature difference between the two

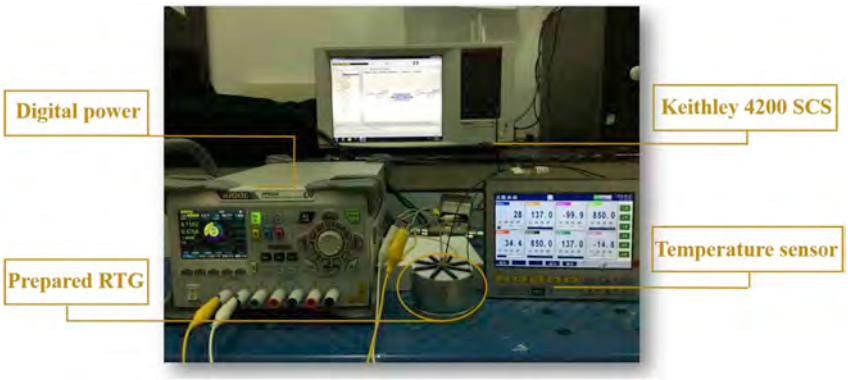

Fig. 3. Electrical test chart of the RTG.

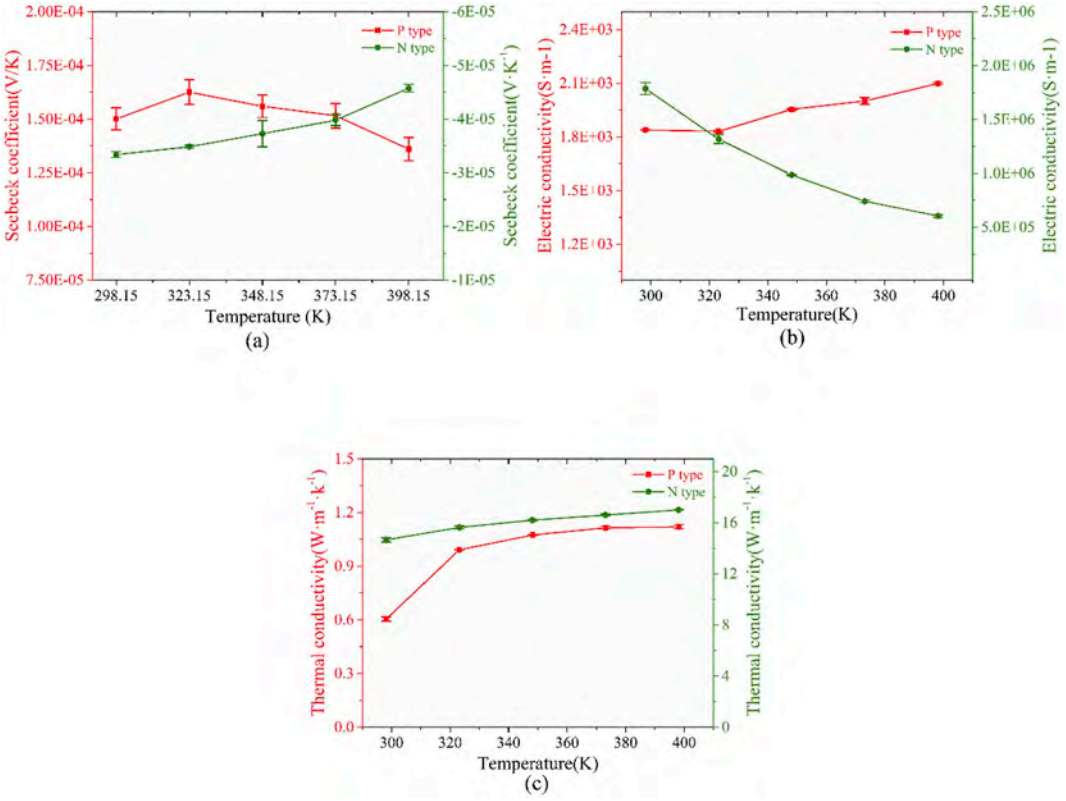

Fig. 4. Material performances of P-/N-type thermoelectric materials with regard to temperature: (a) Seebeck coefficient, (b) electrical conductivity, and (c) thermal conductivity.

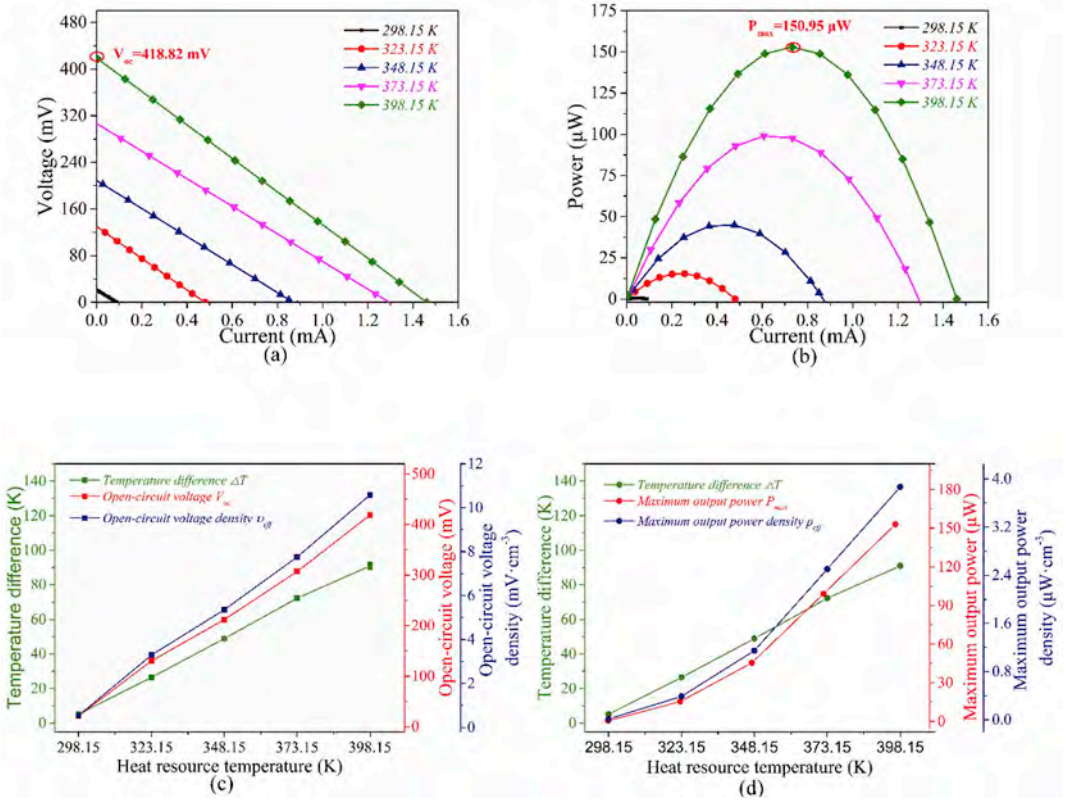

Fig. 5. Prepared miniaturized RTG: (a) *V–I* characteristic curves, (b) Power-Ampere (*P–I*) characteristic curves, (c) ΔT, V_{oc}, and ν_{eff} versus T_h, (d) ΔT, P_{max}, and ρ_{eff} versus T_h.

ends of the filament increases. On the basis of the preceding equations, the output voltage and power of the RTG also increase correspondingly. When T_h is 398.15 K, ΔT between the two ends of the thermoelectric filament is up to 91.0 K. The result shows a large temperature difference that many thermoelectric devices cannot obtain under low-temperature heat source. The RTG obtain 418.82 mV V_{oc} and 150.95 μW P_{max}, that is, realizing the high-quality output of voltage and power simultaneously (Fig. 5a and b). The corresponding ν_{eff} and ρ_{eff} are 10.58 mV cm^{-3} and 3.87 μW cm^{-3}, as shown in Fig. 5c and d, respectively. This application is the first to use concentric thermoelectric filaments in RTGs. In comparison with other RTGs prepared through the respective structures and methods, the miniaturized RTG based on concentric filament architecture has additional competitive advantages. Its performance shows a good linear change in various heat source temperatures, which is consistent with the change trend of the radioisotope battery by using a thermoelectric material as a conversion unit. Therefore, the miniaturized RTG has achieved practical application success, and it can provide power for space apparatus.

4. Simulation optimization and analysis

The electrical output of the RTG could be remarkably improved by increasing the number of thermoelectric filaments. However, to reveal further the intrinsic methods in improving the performance of the RTG, we investigated the approach of optimizing the output performance from the structure and dimension of the thermoelectric filaments. The COMSOL finite element analysis method was used to facilitate this study.

4.1. Simulation feasibility verification

To verify the feasibility of the finite element analysis method, the COMSOL Multiphysics software was utilized to simulate the prepared RTG using the same size and materials. First, the geometry model in COMSOL was established on the basis of the previously prepared dimension of the RTG, as shown in Table 2. Second, the material properties of P-/N-type thermoelectric materials in Section 3.2 were introduced to the corresponding position. Third, the surface temperature of heat source changed within the range of 298.15–398.15 K in solid heat transfer module. The relevant boundary and initial conditions discussed in Section 2 were successively set. Under the coupling of thermodynamic and electrical physical fields, the RTG generated the open-circuit voltage and internal resistance at the two electrodes. Additional electrical parameters were obtained through calculation. The comparison between experimental and simulated output of the RTG at various temperatures are shown in Fig. 6. In the two cases of the experiment and simulation, the difference in several values, such as V_{oc}, P_{max}, ν_{eff}, ρ_{eff}, and ΔT, are not remarkable and the overall trend are consistent. V_{oc} and P_{max} are the macroscopic manifestation of the Seebeck coefficient and electrical conductivity of the thermoelectric materials, and ΔT is the cumulative change of the thermal conductivity. The experimental results agree well with the simulation, that is, not only the macroscopic conformity of the electrical parameters, such as electric voltage and power, in the experiment and simulation but also the mutual coupling results of the Seebeck coefficient, thermal conductivity, and electrical conductivity at the micro level. The finite element analysis method has been proven to simulate the thermoelectric conversion of the RTG accurately, including the establishment of a geometric model, substitution of performance parameters for the thermoelectric materials, and coupling of multiple physical fields. The accurate relationship is established between the object and the model, which laid the foundation of our future optimization research. In comparison with other similar research works that used this finite element analysis method, the present work realizes the weak difference of the electrical parameters between the simulated and experimental values, which are successfully applied in the radioisotope battery. This study also provides a convenient and efficient approach to evaluate RTGs.

4.2. Influence of the L and P-/N-type cross-sectional area on RTG

Based on the analysis in Section 2, the output performance of the RTG was dependent on the size parameters of thermoelectric filaments to a large extent. The present section discussed the influence of the L and P-/N-type cross-sectional area on the performance of the RTG. Firstly, the thickness of the insulation layer was 0.2 mm according to the actual brush painting process. r_3 was set to 1 mm, and r_1 was changed within the range of 0.1–0.7 mm. The ratio of r_1/r_3 reflected the effect of P-/N-type cross-sectional area ratio on the battery performance. Secondly, L varied within the range of 10–50 mm. V_{oc} and P_{max} of the RTG in different r_1/r_3 and L are shown in Fig. 7a and b. When r_1/r_3 is decreased and L is increased gradually, V_{oc} increases. When T_h is 398.15 K, the maximum V_{oc} (i.e., 652.88 mV) occurs at $r_1/r_3 = 0.1$ and $L = 50$ mm. P_{max} increases with the decreases of r_1/r_3 and initially increases and then decreases with the increase of L. This result is caused by the increase in L indicating the increase in l_p and l_n in the thermoelectric filament, leading to an increase in R_r according to Eq. (2). Moreover, the growth rate of R_r begins slowly but gradually exceeds the square of V_{oc} (Supplementary Information 3). Hence, the value of P_{max} initially increases and then decreases according to Eq. (9). When T_h is 398.15 K, P_{max} (i.e., 423.50 μW) occurs at $r_1/r_3 = 0.1$ and $L = 20$ mm. As shown in Fig. 7c and d, ν_{eff} and ρ_{eff} increase with the decrease of r_1/r_3 and L because the increase in volume reduced the density value. The maximum ν_{eff} (i.e., 29.42 mV cm^{-3}) and the maximum ρ_{eff} (i.e.,

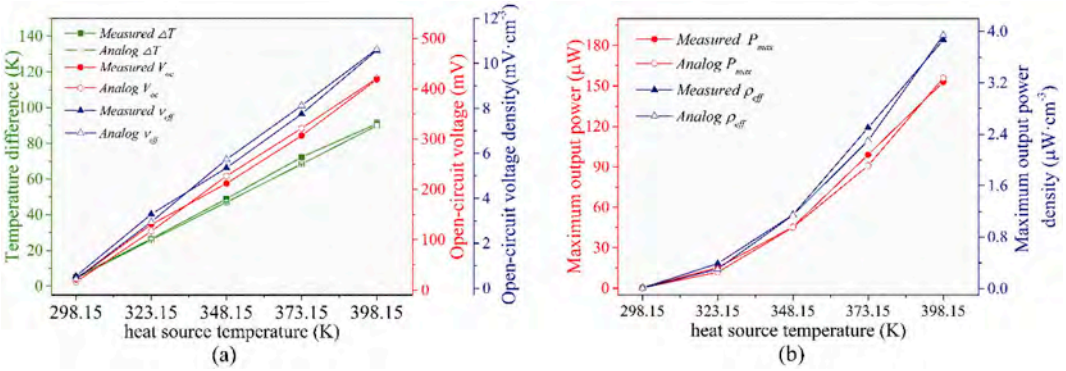

Fig. 6. Comparative analysis of experimental and simulated values for miniaturized RTG. (a) ΔT, V_{oc}, and ν_{eff} versus T_h and (b) P_{max} and ρ_{eff} versus T_h.

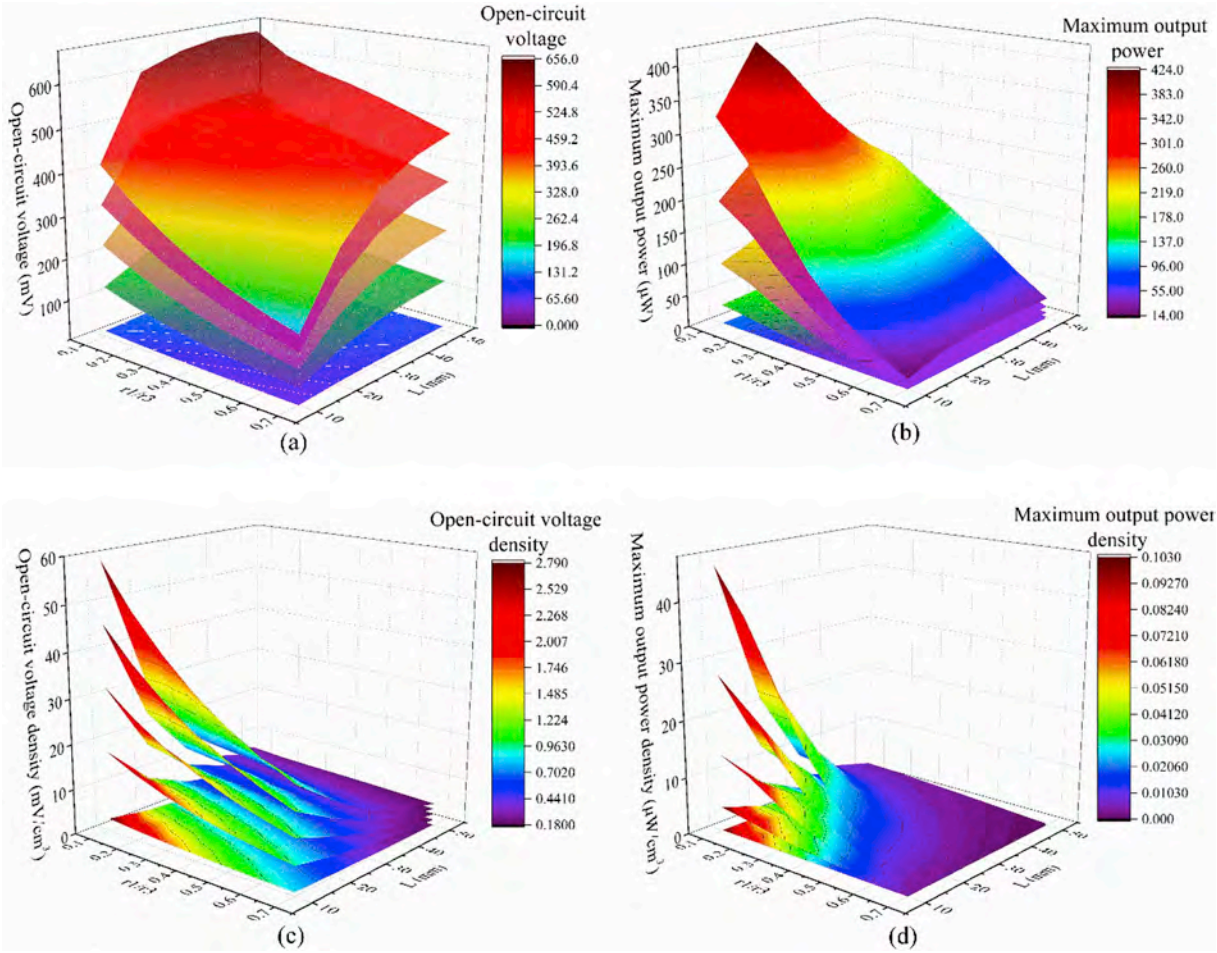

Fig. 7. Electrical performance of the RTG in various sizes: (a) open-circuit voltage V_{oc}, (b) maximum output power P_{max}, (c) effective open-circuit voltage density ν_{eff}, and (d) effective maximum output power density ρ_{eff}.

22.90 W cm^{-3}) are obtained at $r_1/r_3 = 0.1$ and $L = 10$ mm. Based on the output performance and practical application perspectives, we select the output power and the appropriate volume as a preferred principle. Thus, the optimal size of RTG is $r_1/r_3 = 0.1$, $L = 20$ mm (i.e., $r_1 = 0.1$ mm, $r_3 = 1$ mm). Moreover, V_{oc} reaches 605.84 mV.

4.3. Influence of bending degrees on RTG

The output performance of the RTG could be optimized by optimizing the overall volume, which depend in large part on the curving degree of a thermoelectric filament. The thermoelectric filament possessed an excellent strength and flexibility due to the brush paint method and N-type constantan material. Hence, a thermoelectric filament with a certain bending angle could be prepared by brushing the insulating layer and P-type thermoelectric paint on the N-type curving material. Finally, the RTG made from these thermoelectric filaments may have a different diameter/volume and electrical performance. Therefore, the possible influence of the thermoelectric filaments with various bending degrees on the performance of batteries was discussed. First, the best optimal size determined previously ($r_3 = 1$ mm, $r_1 = 0.1$ mm, $L = 20$ mm) was selected as the size of the thermoelectric filament. Then, the curvature (θ) of the thermoelectric filament was changed from 0° to 170° (to avoid the overlap of the thermoelectric filaments), and the thermoelectric conversion process was simulated with T_h in the range of 298.15–398.15 K. The output performance of the RTG vary minimally in various bending degrees, as shown in Fig. 8a and b. When the bending degree increases from 0° to 170°, the voltage and power densities of the RTG gradually increase, as shown in Fig. 8c and d. This result is attributed to the fact that a thermoelectric filament with a large bending degree indicates that it has a small radius and overall volume. Thus, the electrical density is remarkably improved. The radius of the RTG is 16.2 mm at a curvature of 170°. When T_h is 398.15 K, the corresponding ν_{eff} is 73.79 mV cm^{-3} and ρ_{eff} is 53.76 W cm^{-3}. In comparison with the 0° curvature, the voltage and power densities of the RTG are enhanced by 2.4 times. This optimization obtain a small battery volume and improve electrical output, which fully reflect the advantages of the bending properties of the thermoelectric filament.

5. Conclusion

Given the independent and flexible power supply requirements for space apparatus, this study innovatively prepares a miniaturized RTG based on concentric filament architecture. The close relationship between the electrical output and structural size of thermoelectric devices are also discussed. When T_h is 398.15 K, the maximum V_{oc} is 418.82 mV and the maximum P_{max} is 150.95 μW. This result effectively validates that the thermoelectric filament structure has a good practical application in the RTG. The size and volume of RTG are logically optimized on the basis of the finite element analysis method, and the optimal size is $r_1/r_3 = 0.1$ and $L = 20$ mm. When T_h is 398.15 K, the maximum P_{max} is 423.50 μW and the corresponding V_{oc} is 605.84 mV. With the

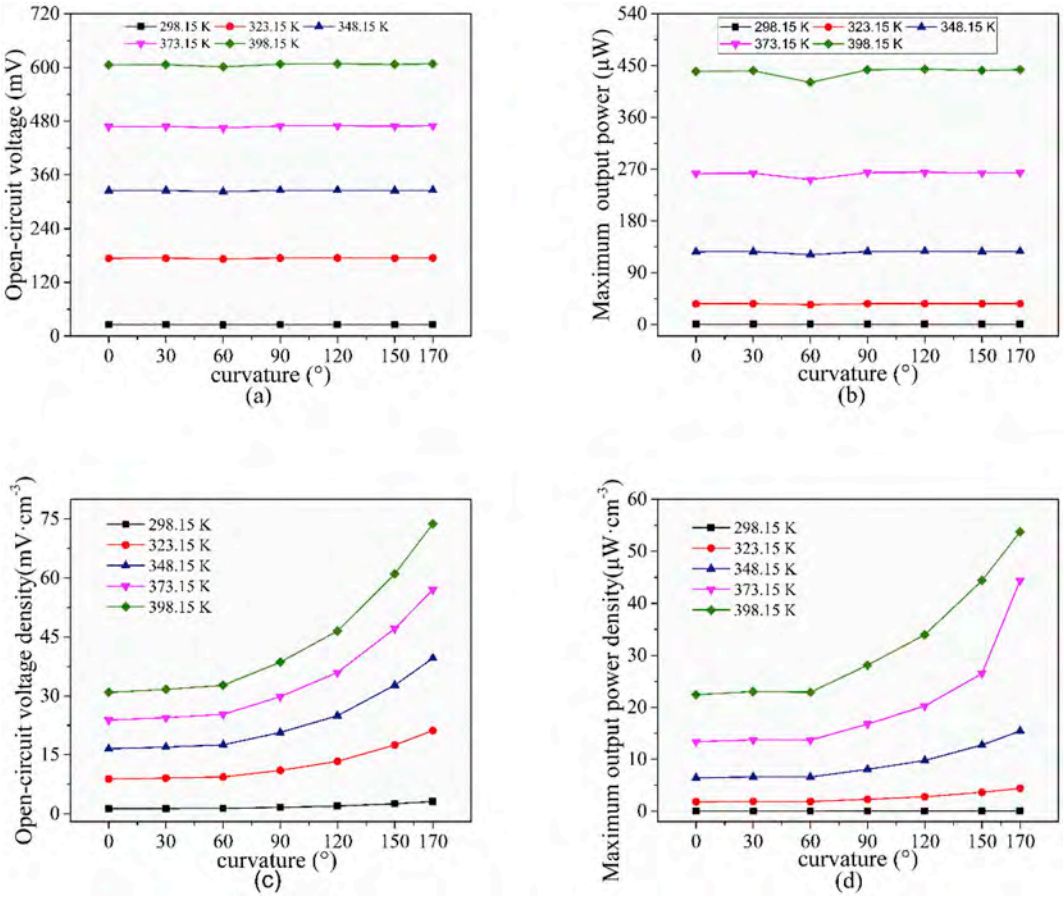

Fig. 8. Electrical performance of the RTG in various curvatures: (a) open-circuit voltage V_{oc}, (b) maximum output power P_{max}, (c) effective open-circuit voltage density ν_{eff}, and (d) effective maximum output power density ρ_{eff}.

increasing curvature of the thermoelectric filament, the overall volume and density of the RTG are remarkably optimized and improved. When the curvature is 170°, ν_{eff} is 73.79 mV cm^{-3} and ρ_{eff} is 53.76 μW cm^{-3}. Hence, providing a practical power support for space microelectronic devices by the proposed miniaturized RTG is possible. The number of thermoelectric filaments in unit volume will be increased to improve further the output performance of the RTG, including increasing the number of thermoelectric filaments in a single module and reducing the volume of unnecessary materials. This work provides a new reference for the preparation and design optimization of miniaturized RTG and support a long-term and sustainable power supply for microelectronic devices, such as space accelerometer, gyroscope, and magnetic sensor.

Acknowledgements

This work was supported by the National Natural Science Foundation of China (Grant Nos. 11675076 and 11505096), the National Defense Basic Scientific Research Project (Grant No. JCKY2016605C006), the Natural Science Foundation of Jiangsu Province (Grant No. BK20150735), and the Jiangsu Planned Projects for Postdoctoral Research Funds (Grant No. 1601139B).

Appendix A. Supplementary data

Supplementary data to this article can be found online at https://doi.org/10.1016/j.jpowsour.2018.10.052.

References

[1] Y.A. Surkov, Scientific instrument making in space exploration, Phys. Usp. 43 (2000) 1017–1019.
[2] L. Summerer, B. Gardini, G. Gianfiglio, Esa's approach to nuclear power sources for space applications, Proceedings of ICAPP, 2007, p. 7325.
[3] F. Ritz, C.E. Peterson, Multi-mission radioisotope thermoelectric generator (MMRTG) program overview, Aerospace Conf. 5 (2004) 2955–2957.
[4] G.R. Schmidt, T.J. Sutliff, L.A. Dudzinski, Radioisotope Power: a Key Technology for Deep Space Exploration, Radioisotopes-applications in Physical Sciences, InTech, 2009.
[5] M.A. Prelas, C.L. Weaver, M.L. Watermann, E.D. Lukosi, R.J. Schott, D.A. Wisniewski, A review of nuclear batteries, Prog. Nucl. Energy 75 (2014) 117–148.
[6] R.W. Drinker, A. Reddy, B. Heshmatpour, G.J. Snyder, K.L. Tuttle, Advanced Superlattice BiTe-PbTe/TAGS Milliwatt Radioisotope Power System, Space Technology & Applications Intforum-sta, 2005, pp. 410–420.
[7] L.A. Flanders, R.W. Drinker, B. Heshmatpour, D.S. Moul, J.P. Fleurial, K.L. Tuttle, Improvements in materials and processes for segmented BiTe/PbTe-BiTe/TAGS/PbSnTe based thermoelectric generators, Space Technology & Applications International Forum-staif, 2005, pp. 564–571.
[8] S.A. Whalen, C.A. Apblett, T.L. Aselage, Improving power density and efficiency of miniature radioisotopic thermoelectric generators, J. Power Sources 180 (2008) 657–663.
[9] W. Glatz, C. Hierold, Flexible micro thermoelectric generator, IEEE International Conference on MICRO Electro Mechanical Systems, 2007, pp. 89–92.
[10] J. Xie, C. Lee, H. Feng, Design, fabrication, and characterization of CMOS MEMS-based thermoelectric power generators, J. Microelectromech. Syst. 19 (2010) 317–324.
[11] Z. Yuan, X. Tang, Z. Xu, J. Li, W. Chen, K. Liu, Y. Liu, Z. Zhang, J. Yan, Screen-printed radial structure micro radioisotope thermoelectric generator, Appl. Energy 225 (2018) 746–754.
[12] K. Liu, X. Tang, Y. Liu, Z. Yuan, J. Li, Z. Xu, Z. Zhang, W. Chen, High-performance and integrated design of thermoelectric generator based on concentric filament architecture, J. Power Sources 393 (2018) 161–168.
[13] M.M. Barry, K.A. Agbim, P. Rao, C.E. Clifford, B.V.K. Reddy, M.K. Chyu, Geometric

optimization of thermoelectric elements for maximum efficiency and power output, Energy 112 (2016) 388–407.
[14] K. Liu, Y. Liu, Z. Xu, Z. Zhang, Z. Yuan, X. Guo, Z. Jin, X. Tang, Experimental prototype and simulation optimization of micro-radial milliwatt-power radioisotope thermoelectric generator, Appl. Therm. Eng. 125 (2017) 425–431.
[15] S. Fan, Y. Gao, Numerical simulation on thermoelectric and mechanical performance of annular thermoelectric generator, Energy 150 (2018) 38–48.
[16] W.H. Chen, S.R. Huang, Y.L. Lin, Performance analysis and optimum operation of a thermoelectric generator by Taguchi method, Appl. Energy 158 (2015) 44–54.
[17] Z.G. Shen, S.Y. Wu, L. Xiao, Theoretical analysis on the performance of annular thermoelectric couple, Energy Convers. Manag. 89 (2015) 244–250.
[18] B.B. Owens, Batteries for Implantable Biomedical Devices, Plenum Press, New York Ny, 1986.
[19] R.C. O'Brien, R.M. Ambrosi, Safe radioisotope thermoelectric generators and heat sources for space applications, J. Nucl. Mater. 377 (2008) 506–521.
[20] T.F. Hursen, S.A. Kolenik, Nuclear energy sources, Ann. N. Y. Acad. Sci. 167 (2010) 661–673.
[21] A. Pustovalov, V. Gusev, A. Borshchevsky, A. Chmielewski, Eighteenth International Conference on Thermoelectrics, (1999), pp. 500–504.
[22] R.E. Bentley, Handbook of Temperature Measurement, Springer, 1998.
[23] V.V. Gusev, A.A. Pustovalov, N.N. Rybkin, L.I. Anatychuk, B.N. Demchuk, I.Y. Ludchak, Milliwatt-power radioisotope thermoelectric generator (RTG) based on plutonium-238, J. Electron. Mater. 40 (2011) 807–811.
[24] A. Pustovalov, Mini-RTGs on plutonium-238: development and application, Eighteenth International Conference on Thermoelectrics, 2002, pp. 509–520.